Characterization of Transfer Functions for Piezoceramic and Conventional Transducers

BOR-TSUEN WANG
Department of Mechanical Engineering, National Pingtung Polytechnic Institute, Pingtung, Taiwan 91207, Republic of China

ABSTRACT: This paper analytically derives the transfer functions for piezoceramic and conventional tranducers and characterizes their relationships in terms of frequency response function (FRF) and modal parameters such as natural frequencies, damping ratios, and mode shapes. The FRFs between accelerometer/point force actuator, accelerometer/PZT actuator, PVDF sensor/point force actuator, and PVDF sensor/PZT actuator are determined, respectively. Those FRFs are expressed in conventional modal model format which can clearly get insight of physical meaning of modal parameters. In particular, the mode shapes of accelerometer, point force actuator, PVDF sensor, and PZT actuator are identified and are proportional to the displacement mode shapes. The point and transfer FRFs are then studied to characterize their properties for either pair of transducer applications. This work leads to the basis for active structural vibration and acoustic control and also draws on ideas for applications of smart structural testing to system identification and diagnosis.

INTRODUCTION

PIEZOCERAMIC transducers have drawn many interests in the application of active structural vibration and acoustic control. The PZT (Lead-Zirconium-Titanate) ceramics are used for their ferroelectric properties, and are usually applied as control actuators. The PZT dynamic actuation model for beam and plate structures has been developed (Hagood, Chung, and von Flotow, 1990; Dimitriadis, Fuller, and Rogers, 1991; Crawley and de Luis, 1987; Wang and Rogers, 1991; Im and Atluri, 1989), and shows its validity for practical applications. The PVDF (polyfluoride) sheet which is a flexible film can be adhered to the structural surface, serving as a sensor. A strip of PVDF film (Hubbard, 1987; Clark, Fuller, and Wicks, 1991) or the shaped PVDF film (Lee and Moon, 1990) sensor has been developed and applied to structural vibration and acoustic control as well.

Alberts and Colvin (1991) derived the voltage transfer functions between PVDF actuation and sensing layers. They showed that the collocated actuator and sensor system is stable. Collins, Miller, and von Flotow (1991) compared the piezopolymer spatial filters with the conventional point sensor and showed that the distributed sensor can improve the closed-loop performance of a control system. Sun, Liang, and Rogers (1994) measured the electric admittance of PZT sensor/actuators so as to obtain mechanical frequency response function of a structure. The structural natural frequency, modal damping, and curvature mode shapes can be properly extracted.

The FRF is interesting in control applications as well as structural modal testing. This paper is to derive the transfer functions between piezoceramic tranducers, such as PZT actuators and PVDF film sensors, and conventional transducers, such as point force actuators and accelerometers. The frequency response functions (FRFs) between accelerometer/point force accelerometer/PZT actuator, PVDF sensor/point force actuator, and PVDF sensor/PZT actuator are respectively derived and expressed in a concise and meaningful modal model format. The individual mode shape of accelerometer, point force actuator, PVDF sensor, or PZT actuator are respectively identified and shown for their orthogonality properties. The orthogonal pairs of mode shapes lead to the physical interpolation of FRFs and result in the theoretical feasibilty of structural modal testing by using any combination of piezoceramic and conventional transducers. The point and transfer FRFs are then numerically shown and demonstrated for their characteristics.

THEORETICAL ANALYSIS

Lateral Vibration of Uniform Beam

Consider a uniform simply-supported beam with length of L, as shown in Figure 1, the equation of motion can be obtained as follows:

$$E_b I \frac{\partial^4 w}{\partial x^4} + \varrho_b b t_b \frac{\partial^2 w}{\partial t^2} = p(x,t) \qquad (1)$$

where E_b is the Young's modulus of the beam, I the moment of inertia, ϱ_b the beam density, t_b the beam thickness, b the beam width, and $p(x,t)$ the force function. The boundary conditions for a simply-supported beam are

Editorial Advisory Board Member: Dr. Robert L. Clark, Jr.

1045-389X/96/04 0390-09 $10.00/0

$$M(0,t) = M(L,t) = E_b I \frac{\partial^2 w}{\partial x^2} = 0 \tag{2}$$

$$w(0,t) = w(L,t) = 0 \tag{3}$$

For free vibration analysis, i.e., $p(x,t) = 0$, the natural frequencies can be found to be

$$\omega_n = (n\pi)^2 \sqrt{\frac{E_b I}{\varrho_b b t_b L^4}} \tag{4}$$

The general form of beam lateral displacement, while the beam is subjected to harmonic inputs, can be written as follows:

$$w(x,t) = e^{i\omega t} \sum_{n=1}^{\infty} W_n \sin \varkappa_n x \tag{5}$$

where

$$\varkappa_n = \frac{n\pi}{L} \tag{6}$$

$$W_n = \frac{P_n}{\varrho_b b t_b (\omega_n^2 - \omega^2)} \tag{7}$$

Here, ω is the excitation frequency; $\varkappa_n$ is the modal number; W_n is the modal amplitude; and P_n is the modal force depending on the forms of external forces. For a harmonic point force with the amplitude of F located at x_f acting on the beam, the force function, $p(x,t)$, can be written as follows:

$$p(x,t) = F\delta(x - x_f)e^{i\omega t} \tag{8}$$

The Delta function, $\delta(x)$, is employed to represent the location of the point force. The modal force, P_n^f, due to the point force excitation is given as follows:

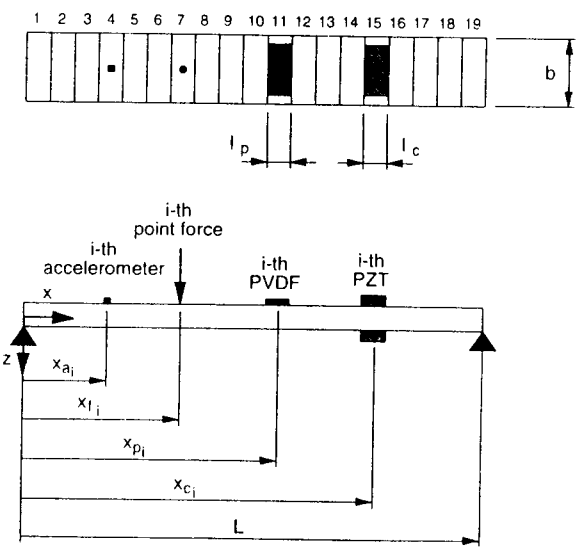

Figure 1. *The arrangement and coordinates of simply-supported beam.*

$$P_n^f = \frac{2F}{L} \sin \varkappa_n x_f \tag{9}$$

where the superscript f signifies the point force. For an actuator consisting of two identical piezoceramic patches bonded symmetrically on the two opposite beam surfaces and activated 180° out-of-phase, the equivalent external forces can be derived as follows (Wang and Rogers, 1991):

$$p(x,t) = K_c V_c [\delta'(x - x_1) - \delta'(x - x_2)] e^{i\omega t} \tag{10}$$

where K_c is some constant depending on physical properties of beam and PZT (Wang and Rogers, 1991; Crawley and de Luis, 1987); V_c is the applied voltage; and $K_c V_c$ is the concentrated moment acting on both edges of piezoelectric patches represented by the first derivative of Delta function. The corresponding expression of modal force for PZT excitation, P_n^c, can be derived as follows:

$$P_n^c = K_c V_c \varkappa_n \sin(\varkappa_n l_c/2) \frac{2}{L} \sin \varkappa_n x_c \tag{11}$$

where x_c and l_c are the central location and the length of the PZT actuator as shown in Figure 1.

PVDF Sensor's Equation

For a PVDF film arranged as shown in Figure 1, the shape function can be expressed as follows:

$$\Gamma(x) = u(x - x_p - l_p/2) - u(x - x_p + l_p/2) \tag{12}$$

where $u(x)$ is the step function; x_p and l_p are the central location and the length of the PVDF film, respectively. The sensor's equation can then be derived as follows (Hubbard, 1987):

$$q(t) = \frac{t_b + t_p}{2} b_p e_{31} \int_0^L \Gamma(x) \frac{\partial^2 w}{\partial x^2} dx \tag{13}$$

$$V_p(t) = \frac{q(t)}{\epsilon A} t_p \tag{14}$$

where b_p is the sensor width, t_p is the sensor thickness, e_{31} is the piezoelectric field intensity constant, ϵ is the permittivity of PVDF films, and A is the sensor area. By substituting $w(x,t)$ and integrating over the beam length, one can obtain the generated voltages $V_p(t)$ as:

$$V_p(t) = e^{i\omega t} \sum_{n=1}^{\infty} W_n K_p \varkappa_n \sin(\varkappa_n l_p/2) \sin \varkappa_n x_p \tag{15}$$

K_p is some constant related to the physical properties of beam and PVDF. It is noted that the generated voltage is proportional to the slope difference between the two edges of a PVDF film (Hubbard, 1987).

Derivation of Frequency Response Functions

By harmonic analysis and by employing the proportional viscous damping model, the frequency response functions between each pair of accelerometer/point force actuator, accelerometer/PZT actuator, PVDF sensor/point force actuator, and PVDF sensor/PZT actuator can be derived as follows:

$$\alpha_{a_i f_j}(\omega) = \frac{x_{a_i}}{F_j} = \sum_{n=1}^{\infty} \frac{\phi^a_{ni}\phi^f_{nj}}{\varrho_b b t_b[(\omega_n^2 - \omega^2) + i(2\xi_n\omega_n\omega)]} \quad (16)$$

$$\alpha_{a_i c_j}(\omega) = \frac{x_{a_i}}{V_{c_j}} = \sum_{n=1}^{\infty} \frac{\phi^a_{ni}\phi^c_{nj}}{\varrho_b b t_b[(\omega_n^2 - \omega^2) + i(2\xi_n\omega_n\omega)]} \quad (17)$$

$$\alpha_{p_i f_j}(\omega) = \frac{V_{p_i}}{F_j} = \sum_{n=1}^{\infty} \frac{\phi^a_{ni}\phi^f_{nj}}{\varrho_b b t_b[(\omega_n^2 - \omega^2) + i(2\xi_n\omega_n\omega)]} \quad (18)$$

$$\alpha_{p_i c_j}(\omega) = \frac{V_{p_i}}{V_{c_j}} = \sum_{n=1}^{\infty} \frac{\phi^p_{ni}\phi^c_{nj}}{\varrho_b b t_b[(\omega_n^2 - \omega^2) + i(2\xi_n\omega_n\omega)]} \quad (19)$$

where

$$\phi^a_{ni} = \sqrt{\frac{2}{L}} \sin \varkappa_n x_{a_i} \quad (20)$$

$$\phi^f_{ni} = \sqrt{\frac{2}{L}} \sin \varkappa_n x_{f_j} \quad (21)$$

$$\phi^p_{ni} = K_p \varkappa_n \sin(\varkappa_n l_p/2)\sqrt{\frac{2}{L}} \sin \varkappa_n x_{p_i} \quad (22)$$

$$\phi^c_{nj} = K_c \varkappa_n \sin(\varkappa_n l_c/2)\sqrt{\frac{2}{L}} \sin \varkappa_n x_{c_j} \quad (23)$$

The response point is denoted by i, and the driving point is denoted by j. The subscripts and superscripts of a, f, p, and c signify the accelerometer, point force, PVDF, and PZT respectively. The numerator of FRFs which is known as "modal constant" (Ewins, 1986) is the product of two mode shape elements. Equations (20)–(23) neglecting subscripts i and j can be identified as the mode shape functions of accelerometer, point force, PVDF sensor, and PZT actuator, respectively. One can easily demonstrate that those mode shape functions are orthogonal to each other. In particular, ϕ^a_n and ϕ^f_n are orthonormal pairs. This implies that either pair of piezoceramic and conventional transducers for which FRFs are shown in Equations (16)–(19) can be used to perform structural modal testing. Once the frequency response functions are measured, any suitable curve fitting algorithm can be applied to determine the modal parameters including natural frequencies, damping ratios, and mode shapes. It is noted that the formulation is only valid for the conditions in which the central location of distributed actuator and sensor coincides with the location of point actuator and sensor, i.e., $x_{a_i} = x_{p_i}$ and $x_{f_j} = x_{c_j}$.

The transfer functions between the ith point (accelerometer) sensor and the ith distributed (PVDF) sensor based on the jth point force and the jth PZT excitation can be defined as follows, respectively:

$$\alpha_{a_i p_i / f_j}(\omega) = \frac{\alpha_{a_i f_j}(\omega)}{\alpha_{p_i f_j}(\omega)} \quad (24)$$

$$\alpha_{a_i p_i / c_j}(\omega) = \frac{\alpha_{a_i c_j}(\omega)}{\alpha_{p_i c_j}(\omega)} \quad (25)$$

The transfer functions between the jth point force and the jth distributed (PZT) actuator based on the ith point (accelerometer) sensor and the ith distributed (PVDF) sensor can be defined as follows, respectively:

$$\alpha_{f_j p_j / a_i}(\omega) = \frac{\alpha_{a_i f_j}(\omega)}{\alpha_{a_i c_j}(\omega)} \quad (26)$$

$$\alpha_{f_j c_j / p_i}(\omega) = \frac{\alpha_{p_i f_j}(\omega)}{\alpha_{p_i c_j}(\omega)} \quad (27)$$

The block diagram is shown in Figure 2.

NUMERICAL RESULTS AND DISCUSSIONS

A steel beam with length of 0.38 m, width of 0.04 m, and thickness of 2 mm is used in the simulations. The natural frequencies are shown in Table 1. The beam is assumed to be equally divided into nineteen divisions to approximate the continuous structure as shown in Figure 1. The acce-

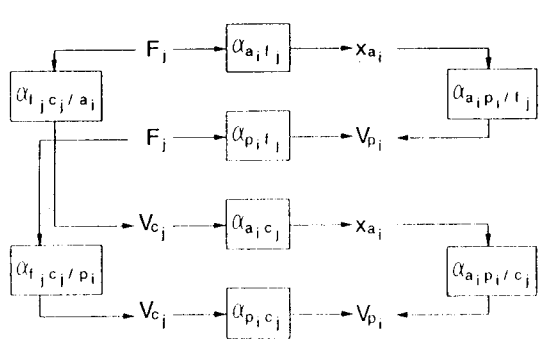

Figure 2. Block diagram of frequency response function.

Table 1. Natural frequencies of the simply-supported beam.

Mode	Frequency (Hz)	Mode	Frequency (Hz)
1	33.2	6	1159.6
2	128.8	7	1578.3
3	289.9	8	2061.4
4	515.4	9	2609.0
5	805.3	10	3220.9

lerometers and point forces are placed at the central location of each division, while the PVDF sensors and PZT actuators are sized with a length of 0.02 m and applied over a full division. The piezoelectric patch (G-1195) (Piezo Systems, 1990) and PVDF films (LDT-28 μk) (Pennwalt Corporation, 1990) are respectively used as the piezoceramic actuator and sensor. Their physical properties are shown in Tables 2 and 3, respectively. The viscous damping ratios are assumed to be 0.01 for all modes. In considering the convergence of series, forty modes are included for numerical simulation. In the following examples, the amplitude and phase angle of the point and transfer FRFs for $i = 2, j = 2$ and $i = 19$, $j = 2$ are shown and plotted over a frequency range of 10–10,000 Hz in logarithmic scale.

The mode shapes of accelerometers, point force, PVDF sensor, and PZT actuators are shown to have the same sinusoidal form for simply-supported beam. They exhibit a different scale. The scaling values depend on the structural modal number and the length of PVDF sensor and PZT actuator as shown in Equations (20)–(23). The first five mode shapes of accelerometer and point forces represented by nineteen points are shown in Figure 3. It is noted that the transducer mode shapes with respect to each type of transducer are proportional to the displacement mode shapes.

Characteristics of Point FRF

Figures 4(a)–4(d) show the point FRFs between actuators/sensors for $i = 2$ and $j = 2$, i.e., the driving point coincides with the response point, corresponding to Equations (16)–(19). As expected, the resonant frequencies agree well for all FRFs, and the antiresonances appear right between resonances. The phase angle plots are also shown. One can observe 180° phase angle changes at each resonance and antiresonance. The first point to notice is that

Table 2. Physical properties of the G-1195 piezoceramic patch (Piezo Systems, 1990).

$E_a = 6.3 \times 10^{10}$ (N/m^2)	$\varrho_a = 7650$ (Kg/m^3)
$t_a = 1.905$ (mm)	$\nu_a = 0.28$
$d_{31} = d_{32} = 166 \times 10^{-12} \left(\frac{\text{m}}{\text{volt}}\right)$	

Table 3. Physical properties of the PVDF films (LDT-28 μk) (Pennwalt Corporation, 1990).

$E_p = 2 \times 10^9$ (N/m^2)	$\varrho_p = 1800$ (Kg/m^3)
$t_p = 28 \times 10^{-6}$ (m)	$\nu_p = 0.33$
$e_{31} = 54 \times 10^{-3}$ (C/m)	$\epsilon = 106 \times 10^{-12}$ (F/m)

α_{af} and α_{pf} have different antiresonance frequencies due to the sign change of modal constant which is the product of mode shape elements. Secondly, α_{af} reveals a mass-dominated characteristic which tends to drift downward, while α_{pc} shows a stiffness-dominated behavior and tends to drift upward. Finally, at lower frequencies, α_{pc} exhibits relatively small peak at resonances.

It is also noted that from the observation of Figures 4(a)–4(d), the resonance points can be clearly identified. The sharpness of the peak and valley are similar, because the modal damping ratios are assumed to be the same for all modes. This implies that either pair of transducers can be applied for structural modal testing to extract the modal parameters. Natural frequencies, damping ratios, and mode shapes can then be obtained through the curve-fitting procedures, if a column or a row of FRF matrix is available. As indicated previously, the modal constant shown in the numerator of the FRFs is correlated to the mode shape components. The physical meanings of the mode shapes as shown in Equations (20)–(23) can be identified to be proportional to the displacement mode shapes for the case of simply supported beam.

In order to further compare the FRFs, all FRFs are scaled based on the values of α_{af} at 10 Hz and plotted in Figure 5. It is noted that α_{ac} and α_{pf} coincide exactly. This can be explained by the comparison of Equations (17) and (18) in which the modal constants for both FRFs are proportional to each other. α_{af} provides lower gains than α_{pf} at high frequencies, and α_{pf} provides more gains than a_{pc}. This result contradicts that shown by Collins et al. (1991). They showed that the gain of distributed (PVDF) sensor is lower than that

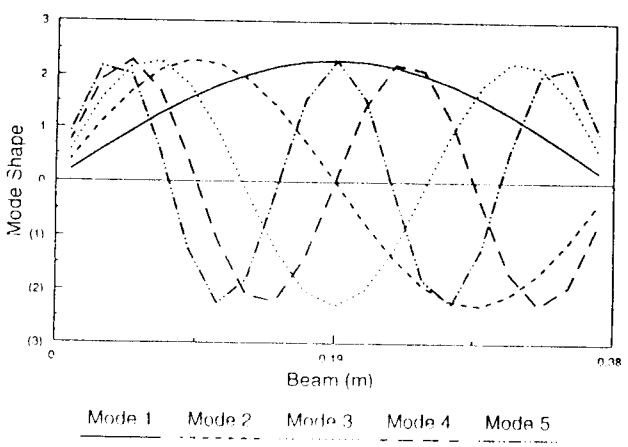

Figure 3. Mode shapes for accelerometer and point force.

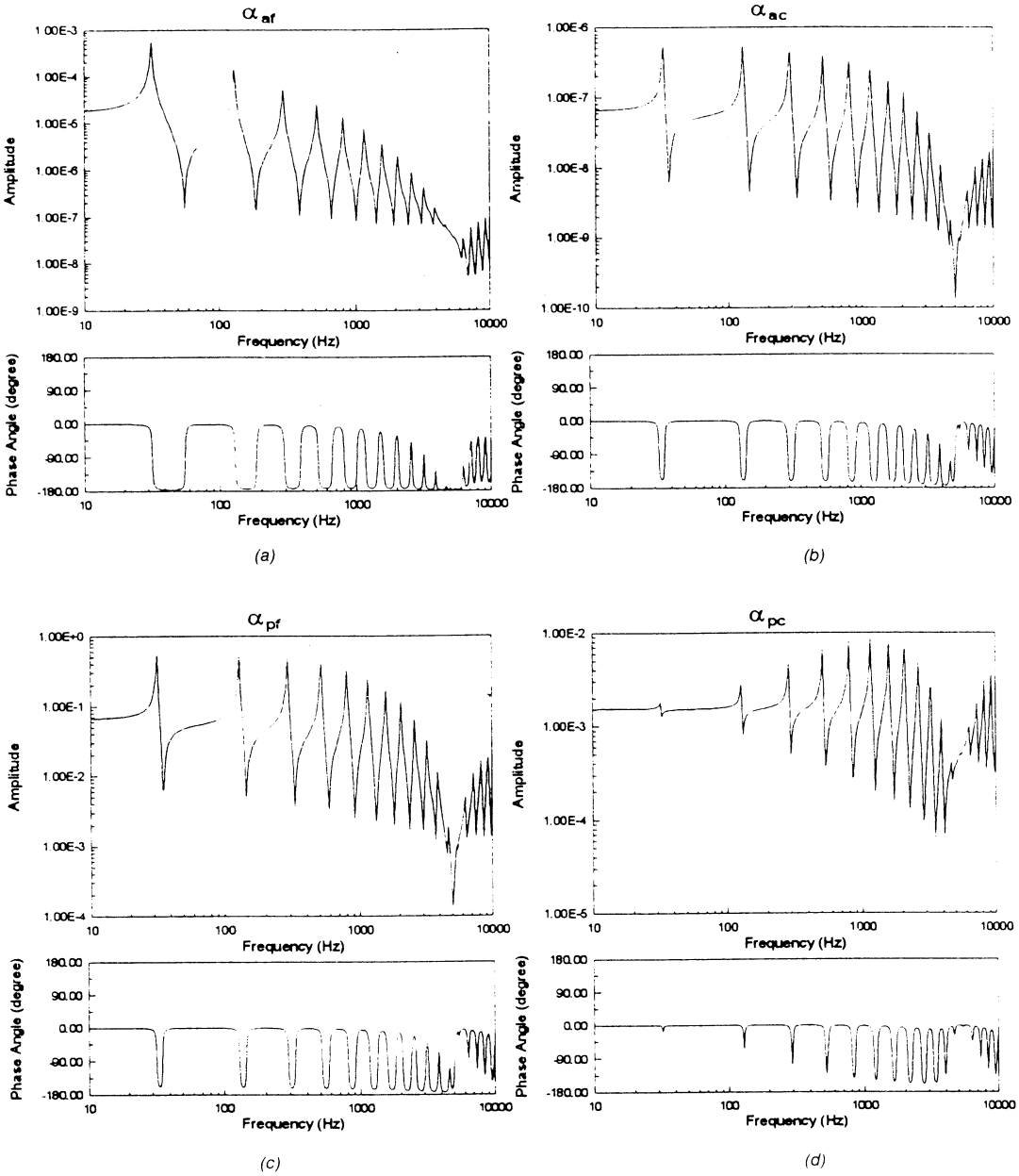

Figure 4. *Point FRF between actuator/sensor for* i = 2, j = 2.

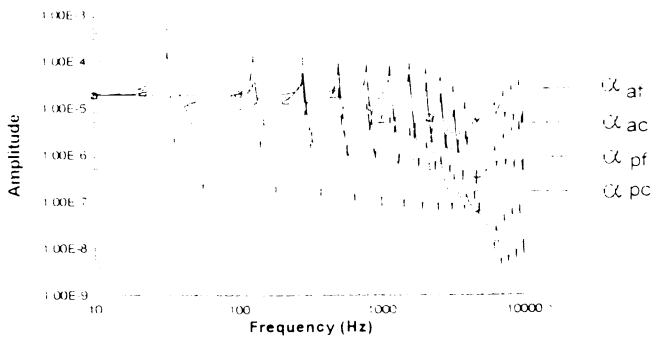

Figure 5. *Comparison of point FRFs between actuator/sensor for* i = 2, j = 2.

of point (accelerometer) sensor at higher frequencies, when the point force excitation is applied.

Figures 6(a) and 6(b) show the transfer functions between accelerometer and PVDF sensor based on the point force excitation and PZT excitation corresponding to Equations (24) and (25), respectively. Both $\alpha_{ap/f}$ and $\alpha_{ap/c}$ reveal resonances and antiresonances. The resonances of $\alpha_{ap/f}$ are right at the antiresonances of α_{pf}, and the antiresonances are at the antiresonances of α_{af}. This can be clearly understood from the FRF equation shown previously. There is phase change at resonance and antiresonance as discussed before. Similar characteristics can be found for $\alpha_{ap/c}$. It is interesting to note that $\alpha_{ap/f}$ and $\alpha_{ap/c}$ reveal quite different resonances and antiresonances, and $\alpha_{ap/f}$ is generally higher than $\alpha_{ap/c}$. This means that PZT actuators can provide more gains than point force actuators in conjunction with the use of either PVDF or accelerometers. It is also noticed that the shapes of $\alpha_{fc/a}$ and $\alpha_{fc/p}$ as shown in Figures 6(c) and 6(d) match exactly with $\alpha_{ap/f}$ and $\alpha_{ap/c}$, respectively, and just have a different scale. This implies that PVDF sensors can provide more gains than accelerometers.

Characteristics of Transfer FRF

Figures 7–9 show the FRFs corresponding to Figures 4–6 except that $i = 19$ and $j = 2$, i.e., the driving point is far away from the response point. This is called the transfer FRF. Similar observations can be made as those discussed

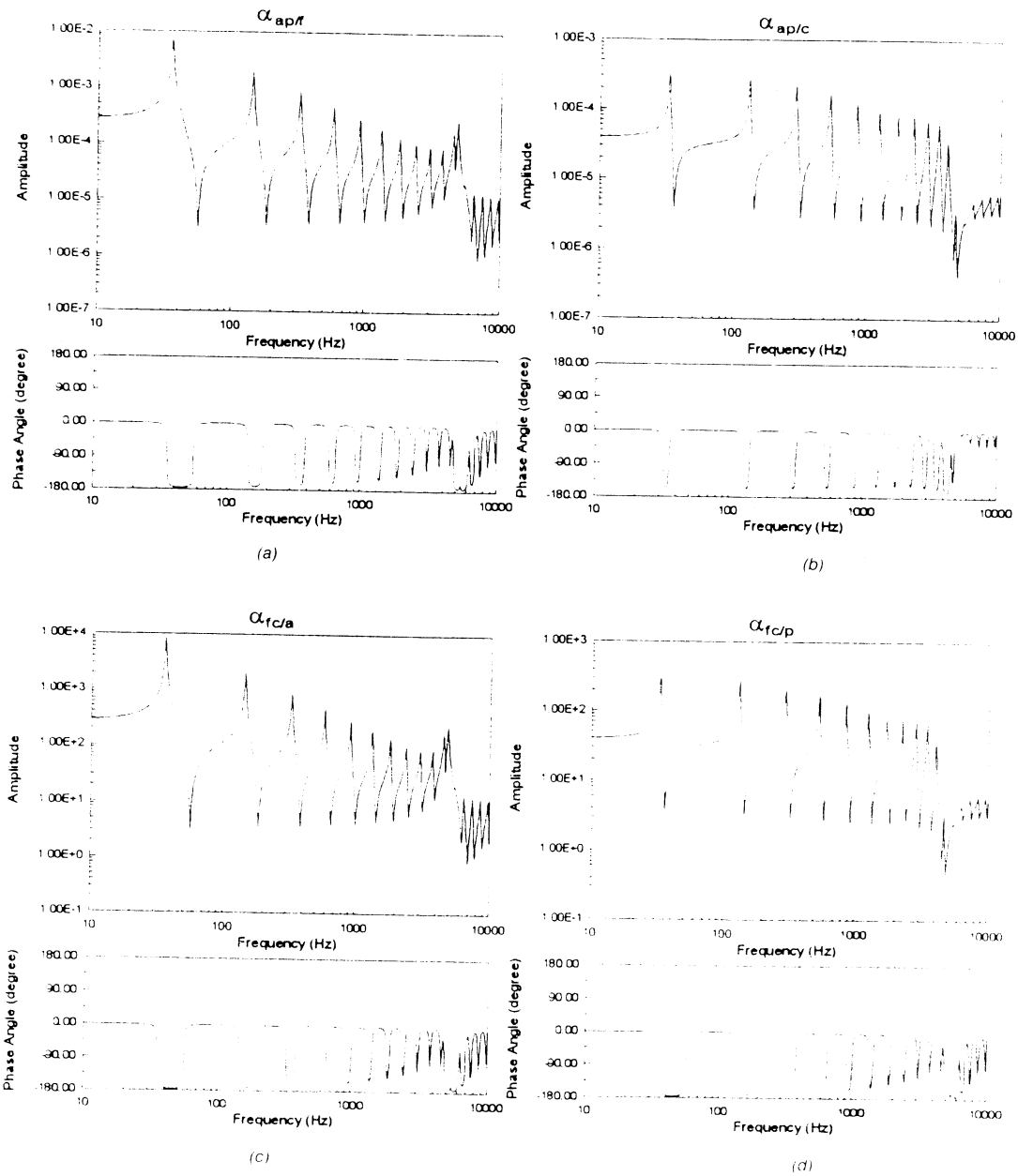

Figure 6. *Point FRF of point/distributed actuator/sensor for i = 2, j = 2*

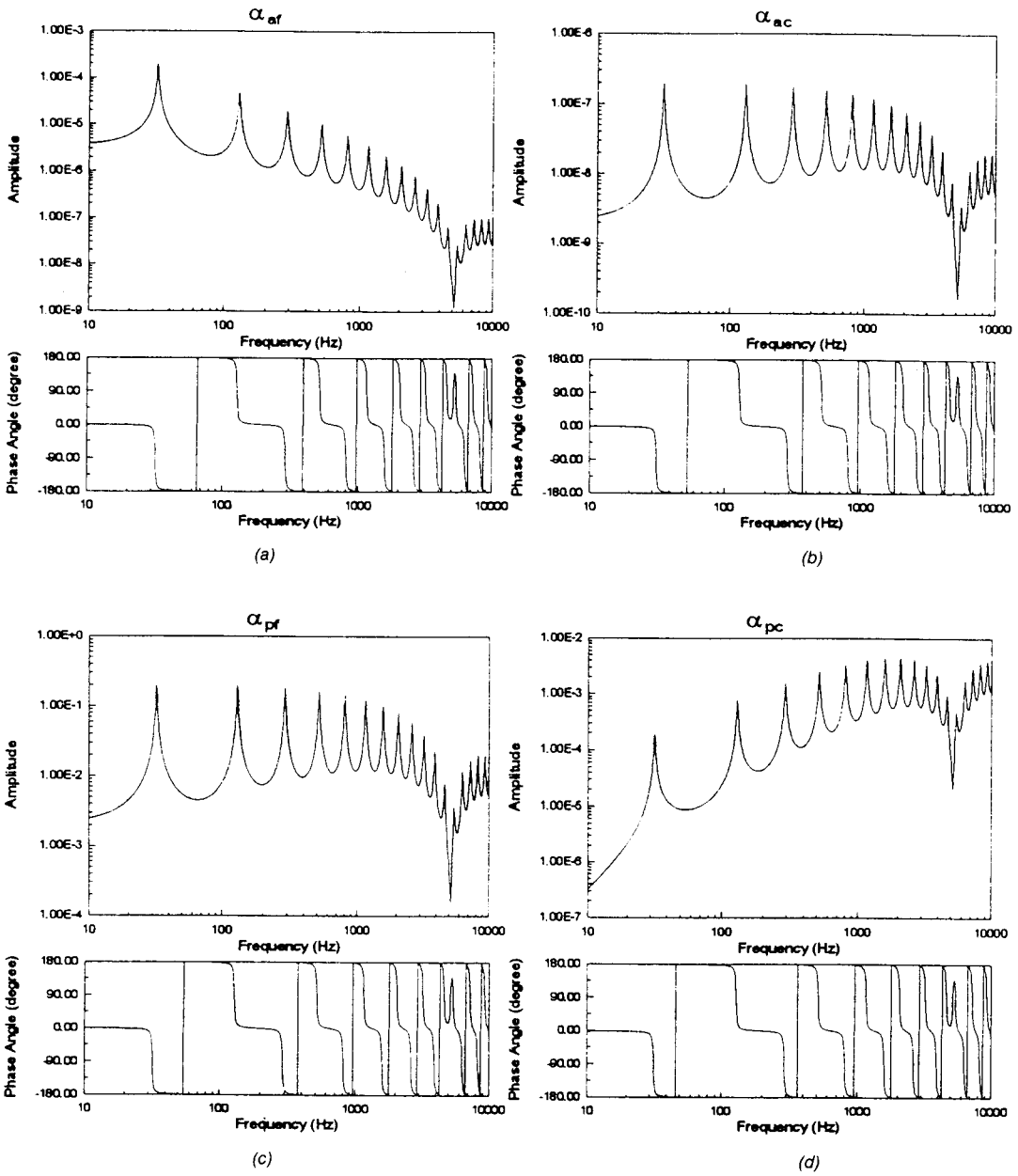

Figure 7. *Transfer FRF between actuator/sensor for* i = 19, j = 2.

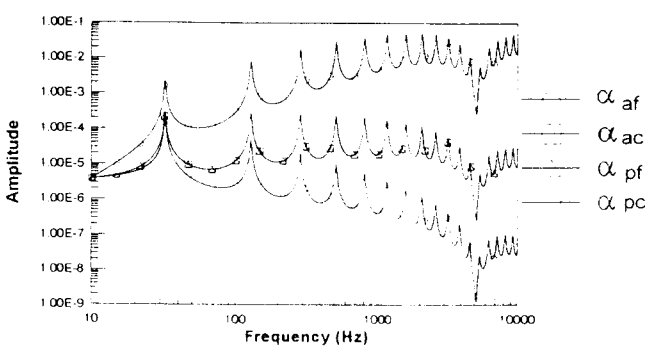

Figure 8. *Comparison of transfer FRF between actuator/sensor for* i = 19, j = 2.

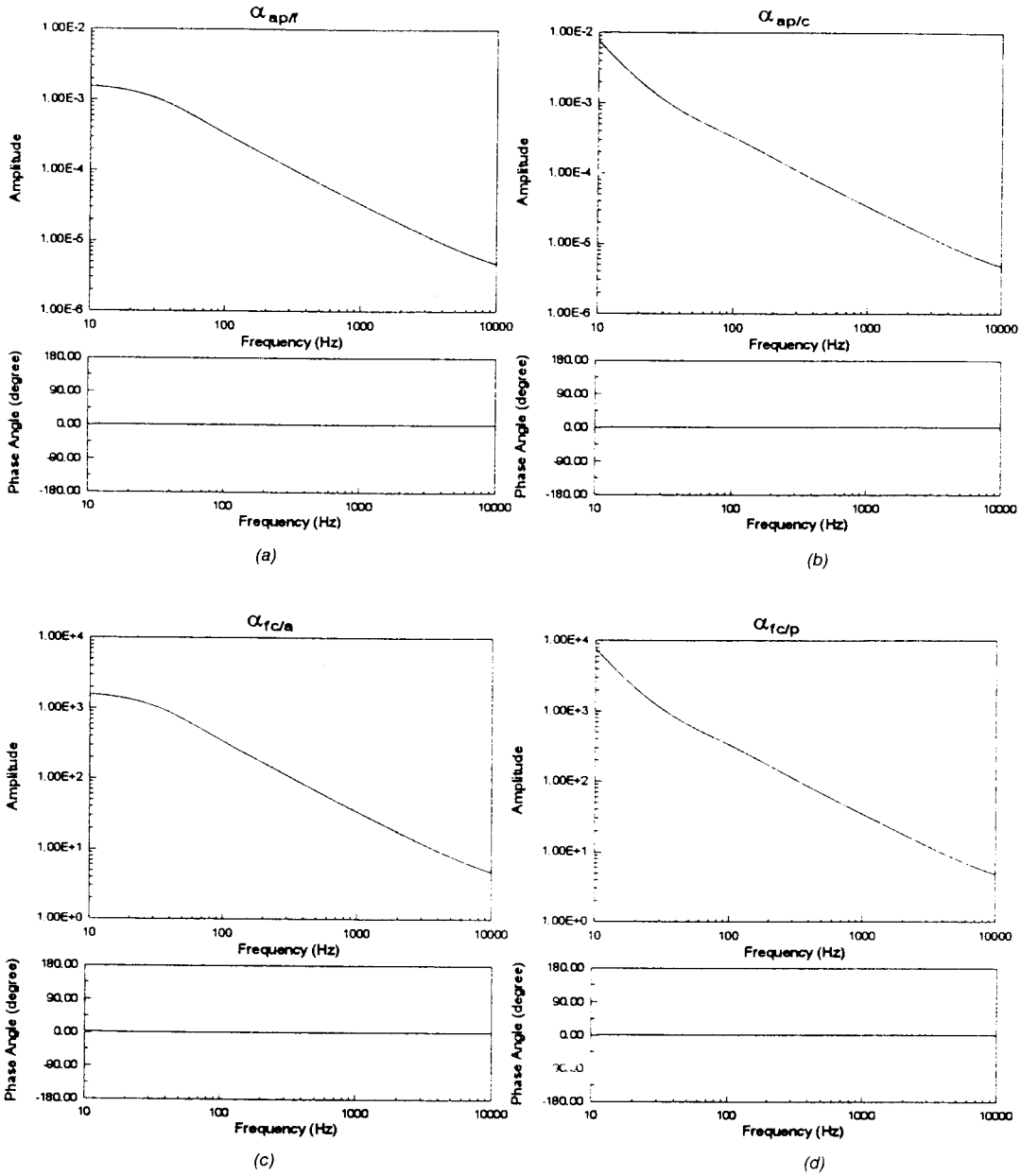

Figure 9. *Transfer FRF of point/distributed actuator/sensor for* i = 19, j = 2.

in point FRFs. The main differences are that there are no antiresonances between resonances, and the phase change may cross over 0° or 180° at the lobe frequencies in Figure 7. Again, α_{af} reveals a mass-dominated characteristic, while α_{pc} shows a stiffness-dominated behavior. Figure 8 again shows all FRFs which are scaled based on the values of α_{af} at 10 Hz. One can observe that the point actuator/sensor can provide more gains than the distributed ones all over the specified frequencies range. Figure 9(a) and 9(b) show the FRFs of $\alpha_{ap/f}$ and $\alpha_{ap/c}$ defined in Equations (24) and (25). One can observe that both FRFs match very well except those frequencies below 30 Hz. This means that when driving point and response point are far enough away, both accelerometer and PVDF sensors result in the same effect for either point or distributed excitation. Also, at higher frequencies, the PVDF sensors provide relatively more gains than the accelerometers.

CONCLUSIONS

This paper characterizes the transfer functions between point/distributed actuators and point/distributed sensors. Four pairs of sensors and actuators, such as accelerometer/-point force actuator, accelerometer/PZT actuator, PVDF sensor/point force actuator, and PVDF sensor/PZT actuator, are investigated. The FRFs are derived and expressed in the modal model format. The individual transducer mode

shape is identified as the displacement mode shape and shows its orthogonality under the conditions that the central locations of distributed actuator/sensor are coincident with those of point actuator/sensor. This implies that the distributed actuator/sensor can be sufficiently utilized for structural modal testing. The modal parameters including natural frequencies, mode shapes, and damping ratios can be obtained by any suitable curve-fitting algorithm, once the FRFs are available. Additionally, the characteristics of point and transfer FRFs are studied. Results show that the distributed actuator/sensor can generally provide more gains than the point actuator/sensor. This work not only draws on ideas for applications of smart structural testing to system identification and diagnosis, but also compares the transfer functions between piezoceramic and conventional transducers leading to active control applications.

REFERENCES

Alberts, T. E. and J. A. Colvin. 1991. "Observations on the Nature of Transfer Functions for Control of Piezoelectric Laminates", *Journal of Intelligent Material Systems and Structures*, 2(4):528-541.

Clark, R. L., C. R. Fuller and A. Wicks. 1991. "Characterization of Multiple Piezoelectric Actuators for Structural Excitation", *Journal of Acoustical Society of America*, 90(1):346-357.

Collins, S. A., D. W. Miller and A. H. von Flotow. 1991. "Piezopolymer Spatial Filters for Active Structural Control", *Proceedings of the Conference on Recent Advances in Active Control of Sound and Vibration*, pp. 219-234.

Crawley, E. F. and J. de Luis. 1987. "Use of Piezoelectric Actuators as Elements of Intelligent Structures", AIAA Journal, 25(10):1373-1385.

Dimitriadis, E. K., C. R. Fuller and C. A. Rogers. 1991. "Piezoelectric Actuators for Distributed Vibration Excitation of Thin Plate", *Journal of Vibration and Acoustics*, 113:100-107.

Ewins, D. J. 1986. *Model Testing: Theory and Practice*, Research Studies Press Ltd., Letchworth, Hertfordshire, England.

Hagood, N. W., W. H. Chung and A. von Flotow. 1990. "Modeling of Piezoelectric Actuator Dynamics for Active Structural Control", *Proceedings of the AIAA/ASME/ASCE/AHS 31st Structures, Structural, Dynamics and Materials Conference*, pp. 2242-2256.

Hubbard, J. E. 1987. "Distributed Sensors and Actuators for Vibration Control in Elastic Components", *Noise-Con 87*, pp. 407-412.

Ims, S. and S. N. Atluri. 1989. "Effects of a Piezo-Actuator on a Finitely Deformed Beam Subjected to General Loading", *AIAA Journal*, 27(12): 1801-1807.

Lee, C. K. and F. C. Moon. 1990. "Modal Sensors/Actuators", *Journal of Applied Mechanics*, 57:434-441.

Pennwalt Corporation. 1990. *Piezo Film Sensor Application Notes*.

Piezo Systems, Inc. 1990. *Product Catalog*.

Sun, F. P., C. Liang and C. A. Rogers. 1994. "Experimental Modal Testing Using Piezoceramic Patches as Collocated Sensor-Actuators", *Proceedings of the 1994 SEM Spring Conference and Exhibits*, pp. 871-879.

Wang, B. T. and C. A. Rogers. 1991. "Modeling of Finite-Length Spatially Distributed Induced Strain Actuators for Laminate Beams Structures", *Journal of Intelligent Material Systems and Structures*, 2(1):38-58.